Experimental investigation of radiation heat waves driven by laser-induced Planck radiation

R. Sigel, G. D. Tsakiris, F. Lavarenne, J. Massen, R. Fedosejevs,* K. Eidmann, J. Meyer-ter-Vehn, M. Murakami,† and S. Witkowski
Max-Planck-Institut für Quantenoptik, D-8046 Garching, Federal Republic of Germany

H. Nishimura, Y. Kato, H. Takabe, T. Endo, K. Kondo, H. Shiraga, S. Sakabe, T. Jitsuno, M. Takagi, and S. Nakai
Institute of Laser Engineering, Osaka University, Suita, Osaka 565, Japan

C. Yamanaka
Institute for Laser Technology, 1-8-4, Utsubohonmachi, Nishiku, Osaka 560, Japan and Himeji Institute of Technology, Himeji, Hyogo 671-22, Japan

(Received 24 July 1991)

The propagation of a radiation heat wave through a thin foil of solid gold was investigated experimentally. The wave is driven by the intense thermal radiation in 1–3-mm-diam gold cavities heated by an intense laser pulse (duration 0.8–0.9 ns, wavelength 0.35 μm) to temperatures ranging from 80 to 240 eV. Evidence of the propagating wave was obtained from the delayed onset of thermal emission from the outer side of the foil. A detailed comparison of the results with the self-similar solution for the ablative heat wave and with numerical simulations is presented.

PACS number(s): 52.50.Jm, 44.40.+a, 47.70.Mc

I. INTRODUCTION

Modern pulsed-power generators, in particular, lasers, make it possible to generate intense, isotropic Planck radiation inside millimeter-size cavities made of high-Z material [1]. With lasers, radiation temperatures up to 240 eV have been achieved [2]. According to the Stéfan-Boltzmann law, the corresponding radiant energy flux exceeds 3×10^{14} W cm^{-2}. The availability of such intense radiation fluxes opens the possibility of investigating the state of matter in a range of temperature and density that was up to now not accessible in the laboratory.

In this work we use laser-generated intense Planck radiation to investigate experimentally the radiation-driven ablative heat wave that forms when intense radiation diffuses into optically dense material. The investigation of this phenomenon is a quite natural first application of laboratory-generated Planck radiation because an ablative heat wave exists also in the wall of a cavity source itself and determines the confinement of the radiation and the cavity temperature. We note that the diffusion of intense radiation into a wall is a classical problem of radiation hydrodynamics [3,4]. For the conditions achievable in the laboratory the radiation heat wave is of the ablative type and can be described by a self-similar solution of the hydrodynamic equations with radiation heat conduction [5].

The principle of the present investigation is shown schematically in Fig. 1. A thin foil made of a high-Z material like gold is exposed on one side to the thermal soft-x-ray radiation generated in a laser-heated cavity. The diffusion of radiation into the foil leads to the formation of a propagating radiation heat wave. As is well known, such a wave has, due to the strong increase of radiation heat conductivity with temperature, a steep front followed by a temperature plateau. When the wave reaches the outer surface of the foil, a sharp onset of radiation towards the outside is expected. From the delay between the switch-on of the cavity source and the onset of radiation from the rear side of the foil, the propagation characteristics of the heat wave can be inferred.

We note that the present work is part of a broader study which also comprises investigation of the radiation temperature and radiation confinement in the cavity [2,6] the exchange of radiative energy between coupled cavities [7], and the propagation of intense radiation through foils of low-Z material [8]. We note also that a short account of the work presented in this paper has been given earlier [9].

II. EXPERIMENTAL SETUP

The scheme of the experiments is shown schematically in Fig. 2. One of two adjacent holes in the cavity wall is covered by a thin gold foil; the other is open and serves as

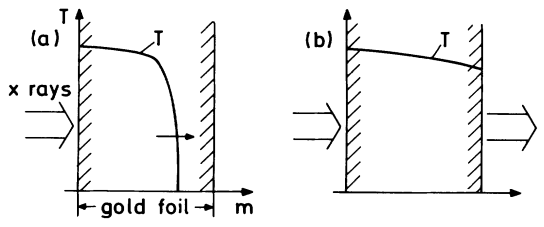

FIG. 1. (a) Propagation of an x-ray-driven radiation heat wave through a thin gold foil; m is the mass coordinate. (b) After arrival of the wave the rear side of the foil emits intense thermal radiation.

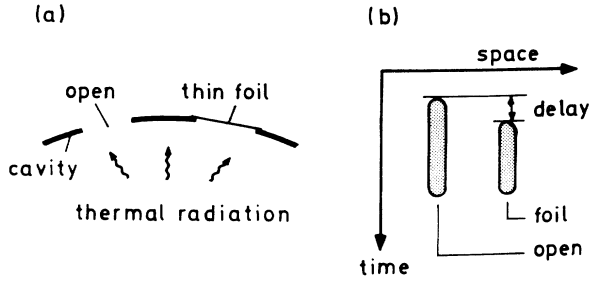

FIG. 2. (a) Experimental scheme. A thin foil is mounted on a diagnostic hole in the cavity wall; a second open hole serves as a reference. (b) Expected signals on the screen of the x-ray streak camera.

a reference hole. The two holes are imaged with spatial resolution onto the photocathode of an x-ray streak camera (XRSC). In the streak mode the camera registers two traces: one measuring the time variation of the cavity radiation, the other that of the foil radiation. From the delay of the latter the transit time of the wave through the foil can be determined.

Three types of cavities ($A-C$) were used in the present study (see Fig. 3). All cavities were made of gold with a wall thickness of 10 μm. The spherical standard cavities of type A (3, 2, or 1 mm diameter) have a hole carrying the foil (f), a reference hole (r), a hole for the measurement of the brightness temperature in the cavity (t), and two opposite laser holes (l) (only one of them is visible in Fig. 3). The cavities of type B (2 or 1 mm diameter) consist of three spherical cavities coupled by the transfer of thermal radiation through large connecting holes. Only the middle cavity is heated by laser light through two opposite laser holes. The upper cavity is nearly closed whereas the lower cavity has large holes (h) and hence is wide open. The main purpose of this design of the type-B cavities is to study radiation confinement by relative measurements between the closed and open satellite cavity [7]. Here we discuss the results of simultaneous measurements of heat-wave propagation through a gold foil mounted on hole (f) on the upper closed cavity. This cavity, in contrast to cavities of type A, is not irradiated by laser light, but is heated only by thermal x rays from

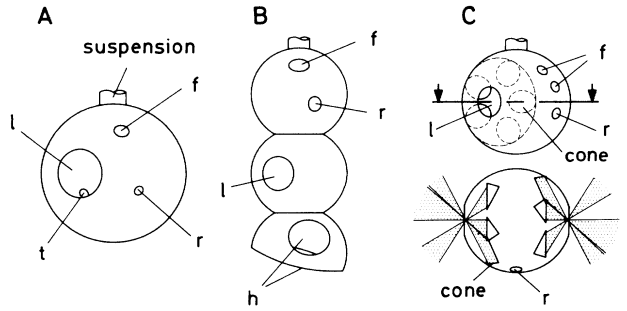

FIG. 3. Cavities of types $A-C$ used in the experiments. Small letters denote the holes with the foil (f), the open reference holes (r), the laser holes (l), the holes for temperature measurement (t), and additional holes (h) in the lower part of the type-B cavity.

the central cavity. Cavity C (diameter 2.5 mm) differs from A in the way the laser light is coupled to the cavity. Behind each of the laser holes the incoming five beams are absorbed inside five hollow gold cones. In the upper view of the target the rim of two of the cones is partially visible through one of the laser holes; the invisible parts of the rims are shown dashed. All these rims of the cones lie in a plane whose intersection line with the spherical cavity is also shown dashed. A cross section through the cavity is marked by the two arrows and shown in the lower view of cavity C (top view). Shown are the three cones located in the lower half of the cavity behind each of the laser holes together with the laser beams heating them. One of the cones on each side is shown open because it lies in the plane of the cross section. The relative positions of these particular cones result from the fact that the two bundles of laser beams are tilted relative to each other around the common axis by an angle $(360°/5)/2=36°$. The apex angle (80°) of the hollow cones (wall thickness 10 μm) and their orientation have been designed in such a manner that any laser light ray, even if located at the periphery of a beam, would after a specular reflection at the inner wall of the cone still fall inside the cone. The heating of the cavity should then proceed as follows: The primary x rays from the laser-produced plasma formed in the cones heat the wall surrounding the laser hole. The central part of the cavity, which carries two holes (f) for the mounting of foils and a reference hole (r), is heated only by re-emitted x rays propagating through the gaps between the cones. In this respect cavity C is similar to the upper closed cavity of target B.

The cavities of types A and B were made by electroplating a single brass mandrel with a 10-μm-thick layer of gold. After etching of the holes through use of a photolithographic technique, the brass was leached out. The target of type C was completed by gluing two partial shells with the laser holes on the main body of the target which had been made together with the cones by the same technique in one piece. With the help of this fabrication technique, targets of very high precision could be made; as an example, Fig. 4(a) shows a scanning electron microscope photograph of a type-A cavity.

The gold foils were fabricated in a series of 40 on a single substrate by electroplating. After electroplating the substrate, the mass per unit area of the gold foil was determined from the weight difference of the substrate (accuracy about 2%). Then photolithographic and etching techniques were applied to fabricate well-defined circular foils. Each foil was reinforced by electroplating a 50-μm-wide by 10-μm-thick gold ring of the required diameter on it. In this way it was possible to obtain well-characterized, flat foils which could be easily handled [see Fig. 4(b)]. The foils were glued onto the hole (f) of the cavity with a layer of glue less than 2 μm thick (great care was taken to keep the actual foil free of glue). The foils were fabricated with diameters (i.e., the inner diameter of the supporting ring) of 250, 150, and 100 μm. The diameters correspond to the diameters of the reference holes in the 3-, 2-, and 1-mm-diam cavities, respectively. The hole carrying the foil had a diameter 50 μm larger

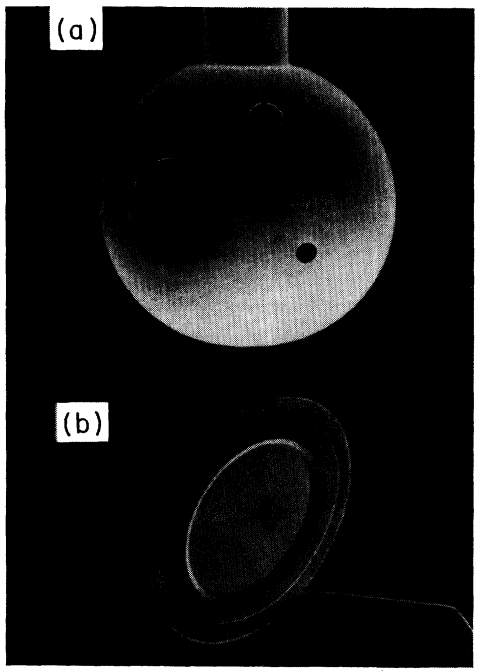

FIG. 4. (a) Scanning electron microscope (SEM) photograph of a type-A gold cavity. Cavity diameter is 2 mm. (b) SEM photograph of a gold foil reinforced by a gold ring (inner ring diameter, 250 μm). Foil and ring are still connected to a supporting foil (which holds all the 40 identical pieces fabricated on a single substrate) from which it will be cut for mounting (fabricated by Dr. Johannes Heidenhain, D-8225 Traunreut, Federal Republic of Germany).

than the foil itself in order to ensure irradiation of the foil over its whole diameter. Foils with a thickness in the range 0.25 to 1.37 μm were used in the experiments.

The technique used to image the pair of holes on the cavity onto the photocathode of the XRSC is illustrated by Fig. 5. With the help of an imaging slit and a second crossed slit carrying a 1000-lines/mm transmission grating, each hole produces a spectrum across the slit of the XRSC. Thus the use of a transmission grating makes it possible to achieve spectral in addition to spatial resolution. The wavelength registered by the XRSC can be adjusted through a lateral shift of the slit carrying the grating. In the following we report measurements made at a wavelength of 60 Å with a spectral resolution of about 6 Å.

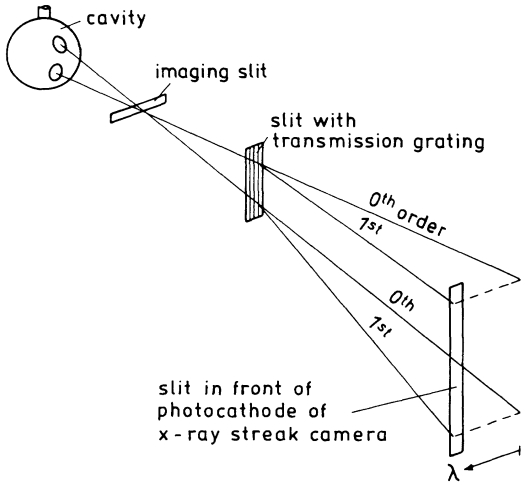

FIG. 5. Setup for imaging of the cavity with spatial and spectral resolution onto the photocathode of the x-ray streak camera.

In addition to the measurements with the XRSC, time-integrated measurements of the spectra emitted by the foil and the reference hole were also made. For this purpose we used a transmission-grating spectrometer (TGS) with absolutely calibrated Kodak 101 film as a detector. The TGS was equipped with a pinhole grating (either 50 or 25 μm in diameter) with 1000 lines/mm and hence provided spectral as well as spatial resolution. A pair of gratings was used in the TGS, one of them covered by a 7.7-μm-thick beryllium foil. With this grating it was possible to obtain very clear spectra in the wavelength range 5–20 Å (the use of a filter suppresses the soft x rays in the zeroth order which tend to blur the spectra in this wavelength range). Photons with these wavelengths are emitted during the most interesting phase when the cavity temperature is high. The cavities were heated with short-wavelength laser light ($\lambda=0.35$ μm) from the Gekko XII Nd-glass laser. Up to ten laser beams, arriving in two bundles of five from opposite sides, injected a mean energy of 358 J per beam into the cavity (the cavities of type B were heated by six beams only). The average pulse duration full width at half maximum (FWHM) was 0.87 ns. Care was taken that the pair of holes was not directly illuminated by laser light nor by first or second reflections (the illumination geometry has been described in more detail in Ref. [6]).

The radiation field in the cavity was investigated in a separate study [6]. At the time of maximum emission the cavity wall was found to radiate with a brightness temperature that depends on the power input and the cavity size. In the present experiments it varied from 80 eV (upper cavity of type-B target) to 240 eV (1-mm type-A cavity). According to the Stéfan-Boltzmann law, this corresponds to a radiant energy flux in the range 4×10^{12} to 3×10^{14} W cm^{-2}. For more details about the cavity radiation, we refer the reader to Ref. [6].

III. EXPERIMENTAL RESULTS

The signals appearing on the screen of the XRSC were registered on Kodak Tri-X film. Figure 6 shows a typical result obtained with a 1.37-μm-thick gold foil on a 1-mm-diam cavity which reached a maximum brightness temperature of 230 eV during the laser heating. The circular screen is surrounded by five fiducial marks. The traces corresponding to the two holes are clearly distinguished. The foil begins to radiate with a delay that amounts to 510 ps in the case shown.

The film images from the XRSC were digitized on a (2D) two-dimensional densitometer and the optical density converted to intensity taking the film characteristics and the geometrical (viewing) factors into account. Figure 7 shows the spectral intensity, at 60 Å radiated by the

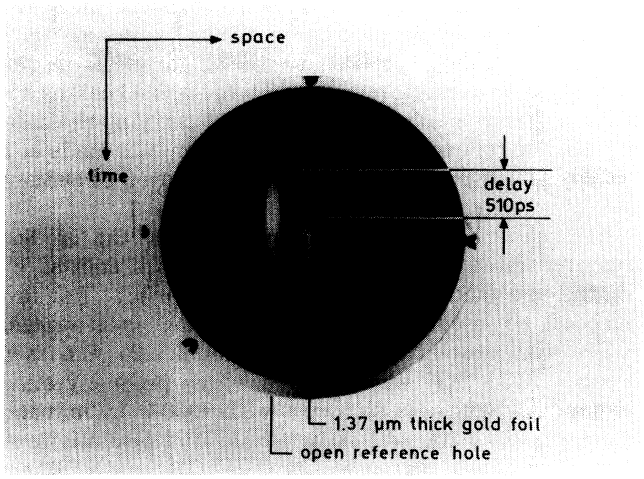

FIG. 6. Screen of the x-ray streak camera showing signals from the gold foil and the open reference hole. Observed wavelength, 60 Å. Cavity temperature, 230 eV. Fiducial marks are seen at the periphery of the screen.

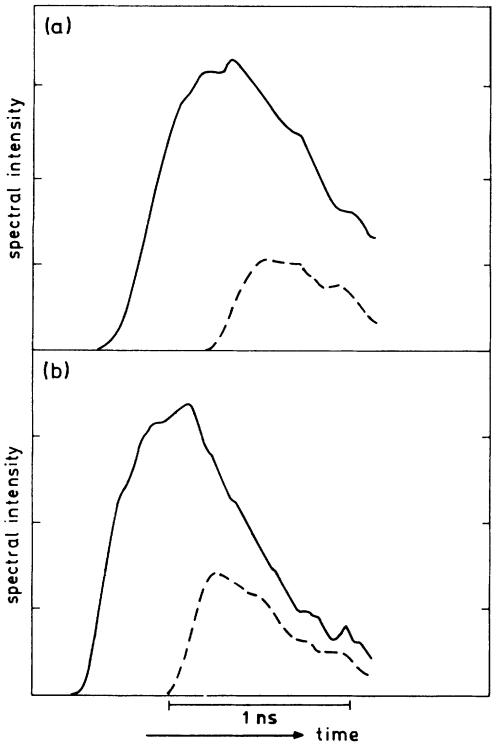

FIG. 7. Measured spectral intensity at 60 Å vs time, radiated by the open reference hole (solid line) and the hole carrying the foil (dashed line). (a) 3-mm type-A cavity irradiated with an incident laser flux $S_L = 6.5 \times 10^{12}$ W cm^{-2}. Gold foil thickness, 0.46 μm. Measured maximum temperature, 96 eV. (b) 1-mm type-A cavity irradiated with an incident laser flux $S_L = 1.7 \times 10^{14}$ W cm^{-2}. Gold foil thickness, 1.37 μm. Measured maximum temperature, 230 eV.

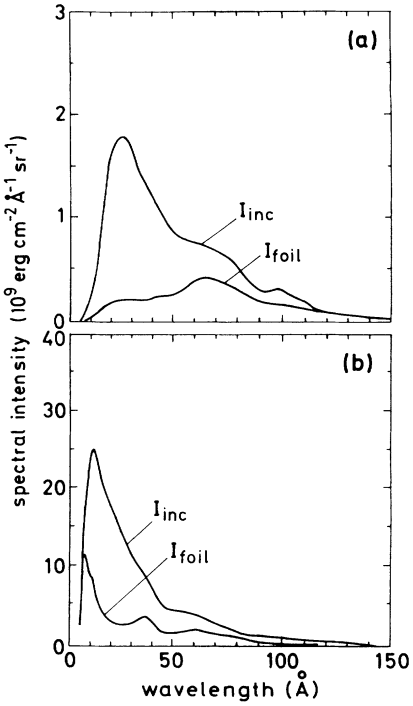

FIG. 8. Measured time-integrated spectra of the radiation observed through the open hole (I_{inc}) and behind the gold foil (I_{foil}). (a) 3-mm cavity; gold foil thickness, 0.36 μm. (b) 1-mm cavity; gold foil thickness, 0.91 μm.

two holes, versus time. Figure 7(a) shows the result from an experiment with a 3-mm-diam cavity of type A heated to a temperature of 96 eV. Foil thickness was 0.46 μm. Figure 7(b) was obtained in the experiment shown already in Fig. 6 (i.e., with a 1.37-μm-thick foil on a 1-mm type-A cavity heated to a temperature of 230 eV). It should be noted that although the overall intensity scale is in arbitrary units in Fig. 7, it is the same for both holes. Thus the ratio of the intensities radiated by the two holes may be taken directly from this figure.

It is remarkable that burn-through was also observed in all experiments with targets of types B and C (only a single experiment with target C was made) in the same manner as was observed in experiments with cavities of type A. This shows clearly that the observed burn-through is not directly a laser-related phenomenon, but an effect due to thermal x rays.

Examples of time-integrated spectra are shown in Fig. 8(a) for a 3-mm-diam cavity and in Fig. 8(b) for a 1-mm-diam cavity. In both cases we have plotted the spectral intensity (I_{inc}) that is incident on the gold foil and observed through the open hole, and the spectral intensity (I_{foil}) observed at the rear side of the gold foil.

IV. DISCUSSION

A. Similarity model

We first discuss the results on the basis of the self-similar solution for the ablative heat wave [5] (similarity model). If a closed cavity made of gold with a density of 19.3 g cm^{-3} is irradiated uniformly by a source flux S_s of

primary x rays (either from the laser-produced plasma in the cavity or from the connecting hole), the scaling laws for the ablative heat wave that forms in the wall as well as simultaneously in the gold foil are

$$d_f = 3.3 S_s^{7/13} t^{10/13} \ \mu\text{m} , \quad (1)$$

$$T = 267 S_s^{4/13} t^{2/13} \ \text{eV} . \quad (2)$$

d_f is the penetration depth and T the temperature. The temporally constant source flux S_s is in units of 10^{14} W cm^{-2} and time t is in units of 10^{-9} s. The scaling laws (1) and (2) are based on the Rosseland opacity for gold calculated in the average-ion approximation [10].

Holes in the cavity cause losses of radiation energy and lower the penetration depth and the temperature in the cavity. The presence of holes can be taken into account by multiplying S_s with a correction factor $1-n^{-1}S_r/S_s$ where n^{-1} is the fractional hole area and $S_r=\sigma T^4$ the flux re-emitted from the hot cavity wall [11]. n^{-1} has the values 0.035, 0.066, and 0.089 for 3-, 2-, and 1-mm cavities of type A and 0.081 and 0.083 for the 2- and 1-mm upper closed cavity of the type-B targets, respectively. For a given value of S_s, S_r and hence the correction factor can be calculated by substituting $T=(S_r/\sigma)^{1/4}$ and solving the implicit equation (2) for S_r. Typical values for the correction factor are 0.92, 0.81, and 0.70 for the 3-, 2-, and 1-mm type-A cavities and 0.85 and 0.79 for the 2- and 1-mm upper closed cavity of the type-B target, respectively.

In Fig. 9 we compare the measured burn-through time with the prediction of the similarity model. The normalized burn-through time shown in Fig. 9 is obtained by dividing the measured time by the time obtained from Eq. (1) for the given parameters of an experiment (namely, S_s, d_f, and, to include hole losses, n^{-1}). The source flux S_s is in fact not directly given but has to be calculated from the incident laser power and the target geometry. In plotting the results obtained with the laser-irradiated cavities of type A, we have assumed that S_s is equal to the incident laser flux S_L, obtained by dividing the injected laser energy through the laser pulse duration and the area of a sphere with the inner diameter of the target. This assumption, which implies that the laser radiation is completely converted into primary source x rays, has been made for simplicity and clarity although it is clearly overoptimistic (see below). The results obtained with the upper, x-ray heated cavity of target B were plotted and evaluated using a calculated value of S_s. It was obtained in calculations of the transfer efficiency from the laser-heated to the upper cavities on the basis of the similarity model as described in Ref. [7]. The experiment made with the type-C cavity was analyzed in a similar manner: The entrance section with the cones was considered as a laser-heated cavity which then couples through the gaps between the cones to the central part of the cavity (the same procedure was used in Ref. [6] for calculating the temperature in this target). Due to the complicated geometry of target C, the results of such calculations must be considered as approximate.

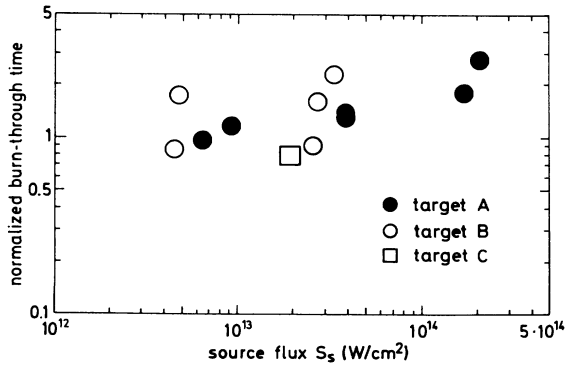

FIG. 9. Comparison of the experimental results with the similarity model. The normalized burn-through time is obtained by dividing the measured time by the time predicted by Eq. (1) for each experiment.

If in Fig. 9 the normalized burn-through time for an experiment is equal to one, this means that the experimentally measured time is in agreement with the prediction of the similarity model. It is seen that the normalized burn-through time is indeed of order unity, for the laser-heated cavities of type A as well as for the x-ray-heated cavities B and C. However, the measurements performed with the type-A cavities over the very large range of nearly two orders of magnitude in S_s also reveal a trend for the normalized burn-through time to increase as the cavities become more strongly heated. This means that the propagation speed of the heat wave becomes lower than predicted. Because the speed of the wave is related to the temperature, this also means that the temperature should be lower than predicted in the upper range.

The investigation of the cavity temperature [2,6] has indeed shown that Eq. (2) overestimates the temperature in the upper range if $S_s=S_L$, i.e., full conversion of the laser radiation in primary source x rays is assumed. Agreement with the measured temperatures was obtained if the decrease of the conversion efficiency with the incident laser flux was taken into account. The decrease in conversion efficiency may also explain the apparent increase of the normalized burn-through time with the flux in Fig. 9 (where $S_s=S_L$ was assumed). This may be seen by noting that, according to Eq. (1), the burn-through time calculated from the similarity model varies with the conversion efficiency $\eta_x=S_s/S_L$ in proportion to $\eta_x^{-7/10}$ and that the conversion efficiency decreases with increasing laser flux. Accordingly, the normalized burn-through time for the two data points at $S_L(=S_s)\approx 2\times10^{14}$ W cm^{-2} in Fig. 9 would be reduced by a factor of 2 (i.e., brought down to one) by assuming a conversion efficiency of $\eta_x=2^{-10/7}=0.4$. This value is not much different from the value of $\eta_x=0.5$ which, in agreement with planar target experiments, was adopted in Refs. [12] and [13], and which leads to good agreement between the measured and calculated temperature. Thus the burn-through measurements and the temperature measurements published elsewhere [2,6] agree, respectively, with Eq. (1) and (2) if allowance for the variation of the conversion efficiency with the laser intensity is made. This is important because we cross-check here two aspects of the

same phenomenon.

Of some concern is the scatter of the data points, especially for the type-*B* targets. It may be partially attributed to the fact that the time of burn-through varies relative to the time of maximum temperature, and pulse-shape effects are not taken into account in the similarity model. However, other causes cannot be excluded. For example, one may speculate that shot-to-shot fluctuations of the energy of the individual laser beams change the spatial distribution of the laser-produced plasma in the central cavity of the type-*B* target which in turn could influence the transfer of x-ray energy through the connecting hole. Unfortunately, little is known at present about the phenomena inside the cavity.

B. Numerical simulations

For a more detailed analysis representative experiments made with type-*A* cavities were simulated in the multigroup diffusion approximation using the MULTI (Ref. [14]) and ILESTA (Refs. [13] and [15]) codes. Such simulations can take into account the real pulse shape, provide a more detailed description of radiative transport (not requiring the assumption of complete thermodynamic equilibrium between radiation and matter), and include the process of laser light conversion into x rays. In the one-dimensional (1D) (spherical) simulations a laser-irradiated gold sphere was located in the center of the cavity. Its surface area was equal to that of the laser-irradiated wall area in the experiment in order to give the correct laser intensity which in turn determines the conversion efficiency and the source spectrum. The thickness of the outer wall was either chosen equal to the foil thickness to simulate burn-through or thick (10 μm) to simulate the evolution of the radiation as seen through the open hole in the experimental cavity. The loss of radiation through holes was taken into account by an appropriate boundary condition at the innermost Lagrangian cell of the wall.

Figure 10 gives the result of simulations of the two experiments shown previously in Figs. 7(a) and 7(b), namely, of an experiment with a 3-mm cavity [Fig. 10(a)] and of an experiment made with a 1-mm cavity [Fig. 10(b)]. A comparison between simulations and experiment reveals agreement in the following respects.

(i) The simulation reproduces the burn-through behavior observed in the experiments in both cases. This is remarkable because the experimental conditions are quite different for the two experiments (S_L was 6.5×10^{12} and 1.7×10^{14} W cm^{-2} for the 3- and 1-mm cavity, respectively).

(ii) The signal radiated by the foil rises somewhat more steeply in the high-intensity case (1 mm cavity).

(iii) The trend in the height of the maximum of the foil signal is reproduced by the simulations. In both the experiments and the simulations, the trend is for the relative height of this maximum (compared to maximum emission through the open hole) to increase if the foil is thin and the cavity temperature high.

(iv) The time of maximum emission through the reference hole advances as conditions change from the 3- to the 1-mm cavity (in the experiment only the time relation between the x-ray signals from different experiments is known, but not the time relation to the laser pulse).

There are also some features of the experiment that are not satisfactorily reproduced by the simulations. Of most concern is that the duration of the x-ray signals is considerably longer in the simulations than in the experiments. The reasons for this discrepancy are unclear at present; they may lie on the experimental or the numerical side. On the experimental side, the most plausible hypothesis is that hole-closure effects [16] tend to cut off the observed radiation with time (this would not explain, however, that the rise time of the x-ray pulse is also shorter in the experiment than in the simulations). This hypothesis is supported by the experimental observation that the emission from the 1-mm cavity decays faster than that from the 3-mm cavity [6], which might be a consequence of the smaller diagnostic hole and higher temperature in the 1-mm cavity. On the theoretical side, possible reasons might be sought in the modeling of the atomic physics of radiative transport, but no convincing hypothesis has been put forward so far (we note that similar difficulties have been encountered in the modeling of x-ray emission from open targets [17]). There is also a trend in the large cavities [compare Figs. 7(a) and 10(a)] for burn-through to occur at a somewhat later time in the simulations than in the experiment. However, because of the wide range

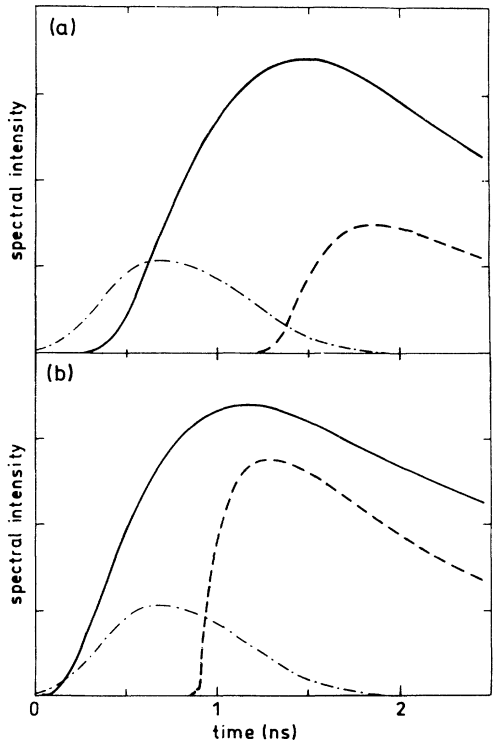

FIG. 10. Spectral intensity at 60 Å radiated by the open reference hole (solid line) and the gold foil (dashed line) from a MULTI simulation. The dashed-dotted line represents the laser pulse shape. (a) 3-mm type-*A* cavity irradiated with an incident laser flux $S_L=6.5\times10^{12}$ W cm^{-2}. Gold foil thickness, 0.46 μm. (b) 1-mm type-*A* cavity irradiated with an incident laser flux $S_L=1.7\times10^{14}$ W cm^{-2}. Gold foil thickness, 1.37 μm.

covered by the experiments, this is considered a minor deviation.

Figures 11(a) and 11(b) show the simulated spatial and temporal evolution of the flux of outward directed photons in the experimentally observed wavelength interval 55–65 Å inside the heated foil. Conditions are the same as in Figs. 7(a) and 7(b) and Figs. 10(a) and (b). As may be seen from a comparison of Figs. 11(a) and 11(b), the profile of the penetrating wave becomes steeper at the front and develops a plateau as the calculated temperature goes up from 90 eV in the 3-mm cavity [Fig. 11(a)] to 220 eV in the 1-mm cavity [Fig. 11(b)]. This is indeed expected because with increasing cavity temperature the amount of heated material and the optical depth of the wave increase and conditions approach complete local thermodynamic equilibrium. In the limit of complete thermodynamic equilibrium, the wave profile will, however, approach that given by the self-similar solution with its characteristic plateau and sharp front. The steepening of the front leads to a sharper rise of the signal radiated by the foil, in the simulations as well as in the experiments.

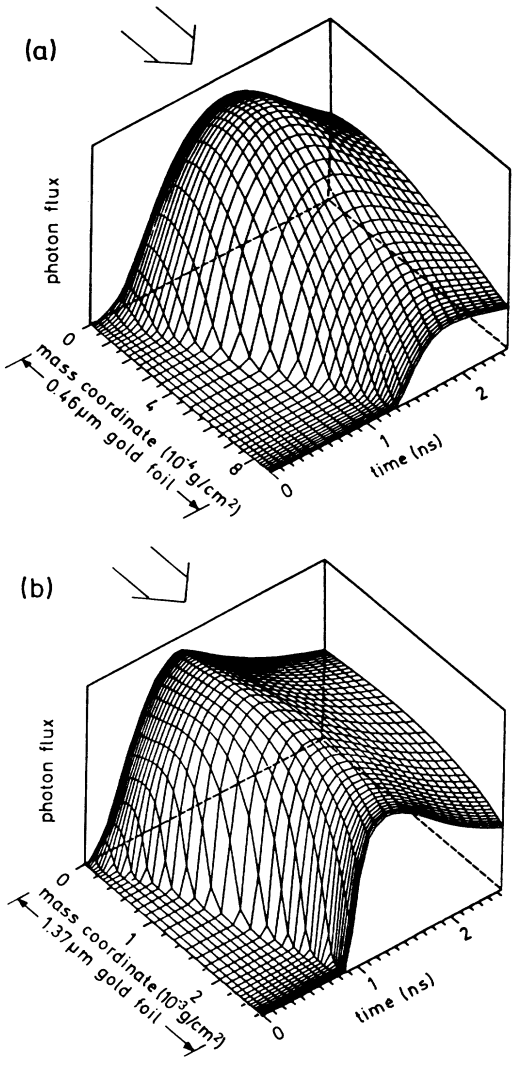

FIG. 11. Evolution of the flux of outward directed photons in the wavelength interval 55–65 Å inside the heated gold foil from a MULTI simulation. Conditions in (a) and (b) are the same as in Figs. 10(a) and 10(b), respectively. The vertical scale is linear.

C. X-ray spectra

In the preceding parts of this paper we have studied the propagation of the radiative heat wave through the optically thick gold foil. As was discussed in Sec. IV A, it could be well described by the similarity model. This model is based on the Rosseland opacity, which is a certain spectral average of the mass absorption coefficient κ_ν. For the calculation of the propagation speed of the radiative heat wave, theoretical values for the Rosseland opacity (taken from Ref. [10]) have been used. The good agreement between the measured and calculated propagation speed of the radiative heat wave gives us confidence that the underlying values for the Rosseland opacity are reasonable.

Beyond that, some information on the spectral dependence of the mass absorption coefficient κ_ν may be obtained from the measured x-ray spectra. Because to our knowledge no direct measurements of κ_ν in hot dense high-Z matter exist, we would like to discuss this aspect in the following.

The time-integrated spectra from the gold foil are generated after the radiative heat wave has propagated through the foil. In this period the whole foil is heated up and in a process of expansion. The hot foil material may no longer be optically thick at all wavelengths and, depending on the value of κ_ν, transmitted light may contribute to the radiation seen by the spectrometer, in addition to the self-emission of the foil.

For an analysis of the measured spectra, consider the situation shown in Fig. 12. Radiation (generated in the cavity) with intensity $I_{\rm inc}$ irradiates the gold foil (denoted as absorber foil) of thickness d. The intensity $I_{\rm foil}$ at the rear side of the foil consists of directly transmitted light I_t and of light $I_{\rm self}$ originating from the self-emission of the heated foil: $I_{\rm foil}=I_t+I_{\rm self}$. If we assume for simplicity that the foil has a spatially homogeneous temperature T_a and mass density ρ_a and also that it is in LTE, then $I_{\rm foil}$ is given by

$$\begin{aligned} I_{\rm foil}&=I_{\rm inc}e^{-\tau}+I_{\rm Pl}(T_a)(1-e^{-\tau})\ , \\ I_t&=I_{\rm inc}e^{-\tau}\ , \\ I_{\rm self}&=I_{\rm Pl}(T_a)(1-e^{-\tau})\ , \end{aligned} \tag{3}$$

where $\tau=\kappa_\nu\rho_a d$ is its optical thickness and $I_{\rm Pl}(T_a)$ the Planck function for its temperature T_a. It is assumed that $I_{\rm foil}$ is measured along the normal of the absorber. I_t is a decreasing and $I_{\rm self}$ an increasing function of τ. Equality ($I_t=I_{\rm self}$) is obtained for

$$\tau=\tau^*=\ln[1+I_{\rm inc}/I_{\rm Pl}(T_a)]\ .$$

The contribution of transmitted light I_t dominates for $\tau\lesssim\tau^*$, whereas for an optically thick foil ($\tau\gg\tau^*$) self-emission dominates. $I_{\rm foil}$ then is given simply by the

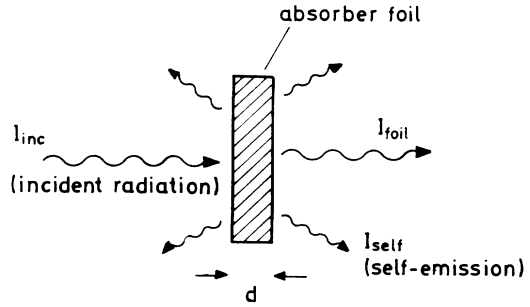

FIG. 12. Scheme for studying the x-ray absorption in radiatively heated matter.

Planck function $I_{Pl}(T_a)$.

The mass absorption coefficient follows from Eq. (3):

$$\kappa_\nu = \frac{1}{\rho_a d} \ln \left[\frac{I_{inc}}{I_{foil} - I_{self}} \right] . \tag{4}$$

Note that the areal mass density ($=\rho_a d$) along the line of sight does not change when the foil expands during heating, provided the expansion is one dimensional. Within this limitation Eq. (4) allows us to determine κ_ν from measured spectra I_{inc}, I_{foil}, and I_{self}.

In the present experiment we were primarily interested in the propagation of the radiative heat wave, and an independent measurement of the self-emission I_{self} has not been made. Therefore, we can deduce from the available data only a lower limit of κ_ν,

$$\kappa_\nu^{lim} = \frac{1}{\rho_a d} \ln \frac{I_{inc}}{I_{foil}} \leq \kappa_\nu , \tag{5}$$

which is obtained by neglecting I_{self} in Eq. (4).

Because no measured data of κ_ν exist for hot gold at all, it is worthwhile to present our experimental results of the lower limit κ_ν^{lim}. Figure 13 shows κ_ν^{lim} as obtained from the spectra shown in Fig. 8 for the 3-mm cavity (dashed curve) and the 1-mm cavity (solid curve). The spatial average of the temperature T_a in the gold foil shortly after burn-through of the radiative heat wave is 100 eV with the 3-mm cavity and 180 eV with the 1-mm

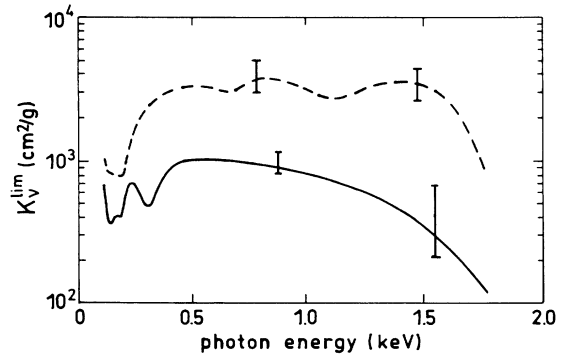

FIG. 13. Lower limit κ_ν^{lim} of the mass absorption coefficient vs photon energy calculated with the help of Eq. (5) from the experimental spectra shown in Fig. 8. Dashed curve, 3-mm cavity [Fig. 8(a)]; solid curve, 1-mm cavity [Fig. 8(b)]. The error bars indicate scattering from different shots.

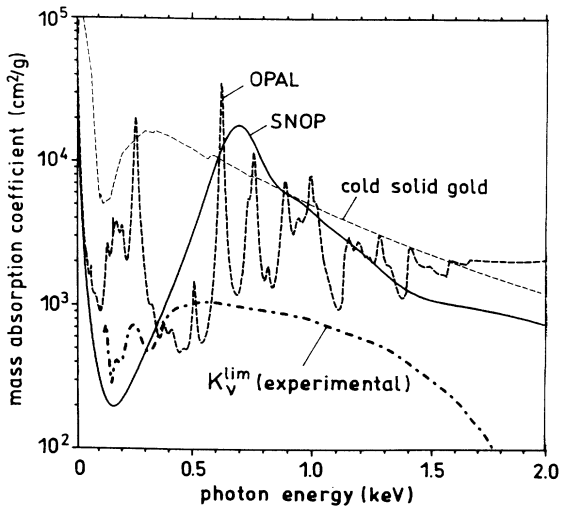

FIG. 14. Mass absorption coefficient of gold as calculated with the SNOP and OPAL models in comparison to the experimental lower limit κ_ν^{lim} at a temperature of 180 eV and a density of 0.1 g/cm^3. The mass absorption coefficient of cold solid gold is also shown.

cavity; the density in both cases is $\rho_a \approx 0.1$ g/cm^3. This follows from hydrodynamic simulations.

It is of interest to compare the experimental κ_ν^{lim} with mass absorption coefficients following from theoretical models and being used in simulations performed with the MULTI hydrocode. Such a comparison is made in Fig. 14 with the SNOP model [18], which describes the atomic level by the principal quantum number only, and with the OPAL model [19], which in addition considers splitting due to the orbital quantum number. The pronounced maximum of the SNOP data for κ_ν at about 0.7 keV is caused by bound-bound transitions of N-shell electrons (no individual lines are visible because a spectral averaging procedure as described in Ref. [18] was applied). The many peaks of the OPAL data for κ_ν are caused by the numerous possible $\Delta n \neq 0$ and $\Delta n = 0$ transitions (no spectral averaging is used in OPAL). In Fig. 14 the mass absorption coefficient of cold solid gold (taken from Ref. [20]) is also shown. Compared to cold gold, the calculated κ_ν of the heated gold plasma is considerably reduced, especially at lower photon energies. This is a consequence of the partial ionization of the outer electron shells of the gold atom.

As one would expect, Fig. 14 shows that the theoretical models are above the experimental lower limit κ_ν^{lim} in most energy regions. An exception is the region 0.1–0.3 keV in case of the SNOP model and the region around 0.5 keV in case of the OPAL model. In these regions the theoretical models seem to underestimate the absorption. This may be an indication that the real κ_ν does not have such pronounced transparency windows (deep minima) between individual lines. This is physically reasonable, because in the complex gold ions many more bound-bound transitions exist than are considered by the simplified models.

We finally note that we have also calculated spectra with the MULTI hydrocode (for details of this type of simulation refer to Ref. [21]). According to Eq. (3), the

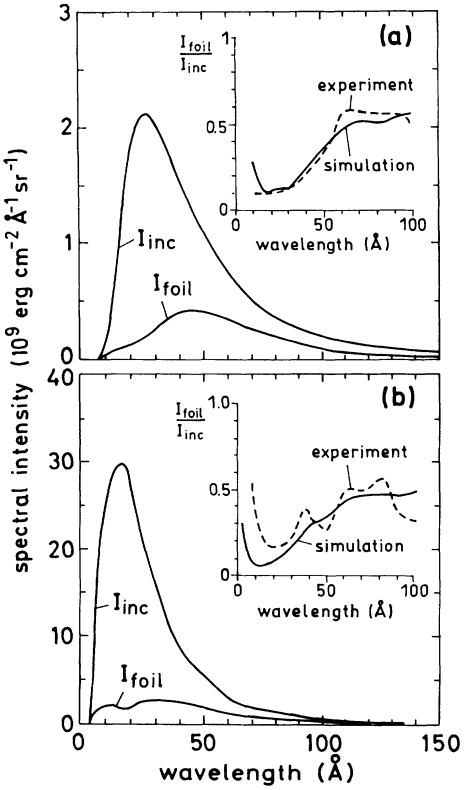

FIG. 15. Simulation of the measured spectra I_{foil} from Fig. 8 with the MULTI hydrocode. The incident radiation I_{inc} was taken for the simulation directly from the experiment (in an approximate form). The insets show the ratio I_{foil}/I_{inc} for comparison of the simulated and measured (Fig. 8) results.

spectra at the rear side of the foil (I_{foil}) contain in general contributions of both transmitted light I_t and self-emission (I_{self}), depending on the spectral variation of κ_ν. Therefore, the shape of the spectra I_{foil} depends on the detailed modeling of κ_ν. This is directly seen in simulations performed with the different atomic physics models SNOP or OPAL (examples are presented in Ref. [21]).

Figure 15 shows simulations (made with the SNOP data for κ_ν) of the experimental spectra shown in Fig. 8. The simulated spectra I_{foil} in Fig. 15 contain considerable contributions of transmitted light at short wavelengths $\lambda \lesssim 10$ Å and in the wavelength band 40 Å $\lesssim \lambda \lesssim 200$ Å where the SNOP value for κ_ν has a pronounced minimum (see Fig. 14). In the other spectral regions, self-emission is dominant, especially in the region 10 Å $\lesssim \lambda \lesssim 40$ Å, where the SNOP κ_ν has a large maximum.

To facilitate the comparison of the calculated spectra with the experimental spectra in Fig. 8, the insets in Fig. 15 show the ratio I_{foil}/I_{inc} for both the experiment and the simulation. It is seen that the simulated spectra reproduce approximately the main trends of the measurement. Remaining deviations are attributed mainly to insufficient accuracy in the modeling of x-ray absorption.

V. SUMMARY

Heat waves play an essential role in radiation hydrodynamics, in particular for the generation of intense Planck radiation under equilibrium conditions. With modern pulsed-power generators such as lasers, they can now be generated and investigated in the laboratory.

In this study we investigated the heat waves driven through a thin foil of gold by the intense thermal radiation formed in a laser-heated cavity. Evidence for the propagating heat wave was obtained from observation of the steep, delayed onset of soft x-ray radiation from the outer surface of the foil. Consistent results were obtained over a wide range (80–240 eV) of the brightness temperature of the radiation in the cavity. In some experiments the cavities were not directly heated by laser light, but the heating energy was injected into the cavity in the form of soft x rays. The results depended only on the heating power but not on the way the cavity was heated, as one expects if the heat wave is driven by the thermal radiation formed in the heated cavity.

The results were compared with the known self-similar solution for an ablative heat wave as well as with numerical simulations. Good agreement with the similarity model was obtained if the intensity dependence of the laser light to x-ray conversion efficiency in the laser heating process of the cavity was taken into account. This is a quite satisfactory result because an independent study performed during the same experimental campaign had shown that the temperature in the cavity is also correctly predicted by the similarity model. The simulations confirm the observations in more detail. A certain discrepancy remains, however, with respect to the time variation of the radiation during the cooling of the cavities.

It is also shown that the spectrum radiated by the heated foil may be used to obtain information about the spectral opacity of the hot foil material. Although the present experiment was not designed for this purpose, it yields a lower limit for the spectral opacity of gold. In the future, laser-heated cavities should become a useful tool for the investigation of matter at high density and temperature.

ACKNOWLEDGMENTS

This work was supported in part by the Commission of the European Communities in the framework of the Euratom—IPP Association and by Monbusho International Scientific Research Program.

*On leave from the Deparment of Electrical Engineering, University of Alberta, Edmonton, Canada T6G 2G7.
†On leave from the Institute of Laser Engineering, Osaka University, Suita, Osaka 565, Japan.

[1] R. Sigel, in *Handbook of Plasma Physics,* edited by M. N. Rosenbluth and R. Z. Sagdeev, Physics of Laser Plasma Vol. 3, edited by A. M. Rubenchik and S. Witkowski (North-Holland, Amsterdam, 1991), pp. 163–197.

[2] R. Sigel, G. D. Tsakiris, F. Lavarenne, J. Massen, R. Fedosejevs, J. Meyer-ter-Vehn, M. Murakami, K. Eidmann, S. Witkowski, H. Nishimura, Y. Kato, H. Takabe, T. Endo, K. Kondo, H. Shiraga, S. Sakabe, T. Jitsuno, M. Takagi, C. Yamanaka, and S. Nakai, in *Proceedings of the Thirteenth International Conference on Controlled Nuclear Fusion Research, Washington, DC, 1990* (IAEA, Vienna, in press), paper IAEA-CN-53/B-2-1.

[3] R. E. Marshak, Phys. Fluids **1**, 24 (1958).

[4] Ya. B. Zel'dovich and Yu. P. Raizer, *Physics of Shock Waves and High-temperature Hydrodynamic Phenomena* (Academic, New York, 1966).

[5] R. Pakula and R. Sigel, Phys. Fluids **28**, 232 (1985); **29**, 1340(E) (1986).

[6] H. Nishimura, Y. Kato, H. Takabe, T. Endo, K. Kondo, H. Shiraga, S. Sakabe, T. Jitsuno, M. Takagi, S. Nakai, R. Sigel, G. D. Tsakiris, J. Massen, M. Murakami, F. Lavarenne, R. Fedosejevs, J. Meyer-ter-Vehn, K. Eidmann, and S. Witkowski, Phys. Rev. A **44**, 8323 (1991).

[7] G. D. Tsakiris, J. Massen, R. Sigel, F. Lavarenne, R. Fedosejevs, J. Meyer-ter-Vehn, K. Eidmann, S. Witkowski, H. Nishimura, Y. Kato, H. Takabe, T. Endo, K. Kondo, H. Shiraga, S. Sakabe, T. Jitsuno, M. Tagaki, C. Yamanaka, and S. Nakai, Phys. Rev. A **42**, 6188 (1990).

[8] T. Endo *et al.* (unpublished).

[9] R. Sigel, G. D. Tsakiris, F. Lavarenne, J. Massen, R. Fedosejevs, J. Meyer-ter-Vehn, M. Murakami, K. Eidmann, S. Witkowski, H. Nishimura, Y. Kato, H. Takabe, T. Endo, K. Kondo, H. Shiraga, S. Sakabe, T. Jitsuno, M. Takagi, C. Yamanaka, and S. Nakai, Phys. Rev. Lett. **65**, 587 (1990).

[10] G. D. Tsakiris and K. Eidmann, J. Quant. Spectrosc. Radiat. Transfer **38**, 353 (1987).

[11] R. Sigel, R. Pakula, S. Sakabe, and G. D. Tsakiris, Phys. Rev. A **38**, 5779 (1988).

[12] P. D. Goldstone, S. R. Goldman, W. C. Mead, J. A. Cobble, G. L. Stradling, R. H. Day, A. Hauer, M. C. Richardson, R. S. Marjoribanks, P. A. Jaanimagi, R. L. Keck, F. J. Marshall, W. Seka, O. Barnouin, B. Yaakobi, and S. A. Letzring, Phys. Rev. Lett. **59**, 56 (1987).

[13] H. Nishimura, H. Takabe, K. Kondo, T. Endo, H. Shiraga, K. Sugimoto, T. Nishikawa, Y. Kato, and S. Nakai, Phys. Rev. A **43**, 961 (1991).

[14] R. Ramis, R. F. Schmalz, and J. Meyer-ter-Vehn, Comput. Phys. Commun. **49**, 475 (1988).

[15] H. Takabe, M. Yamanaka, K. Mima, C. Yamanaka, H. Azechi, M. Miyanaga, M. Nakatsuka, T. Jitsuno, T. Norimatsu, M. Takagi, H. Nishimura, M. Nakai, T. Jabe, T. Sasaki, K. Yoshida, K. Nishihara, Y. Kato, Y. Izawa, T. Yamanaka, and S. Nakai, Phys. Fluids **31**, 2884 (1988).

[16] R. J. Harrach, Rev. Sci. Instrum. **57**, 2192 (1986).

[17] W. C. Mead, E. K. Stover, R. L. Kauffmann, H. N. Kornblum, and B. F. Lasinski, Phys. Rev. A **38**, 5275 (1988).

[18] K. Eidmann, in *Inertial Confinement Fusion,* Proceedings of the Course and Workshop of the International School of Plasma Physics "P. Caldirola," Varenna, 1988, edited by A. Caruso and E. Sindoni (Editrice Compositori, Bologna, Italy, 1989), p. 65.

[19] A. Rickert and J. Meyer-ter-Vehn, Laser Part. Beams **8**, 715 (1990).

[20] B. L. Henke, P. Lee, T. J. Tanaka, R. L. Shimabukuro, and B. K. Fujikawa, At. Data Nucl. Data Tables **27**, 1 (1982).

[21] K. Eidmann, E. M. Lanig, W. Schwanda, R. Sigel, and G. D. Tsakiris, in Industrial and Scientific Uses of High-Power Lasers, The Hague, 1991, edited by J. P. Billon and E. Fabre [Proc. SPIE **1502**, 320 (1991)].

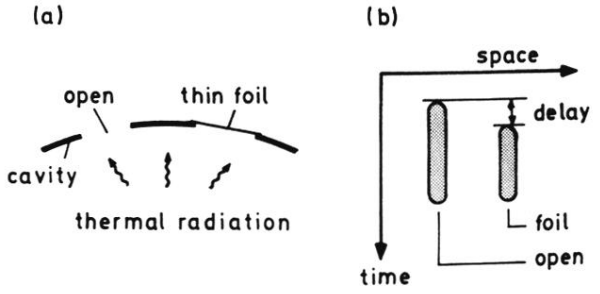

FIG. 2. (a) Experimental scheme. A thin foil is mounted on a diagnostic hole in the cavity wall; a second open hole serves as a reference. (b) Expected signals on the screen of the x-ray streak camera.

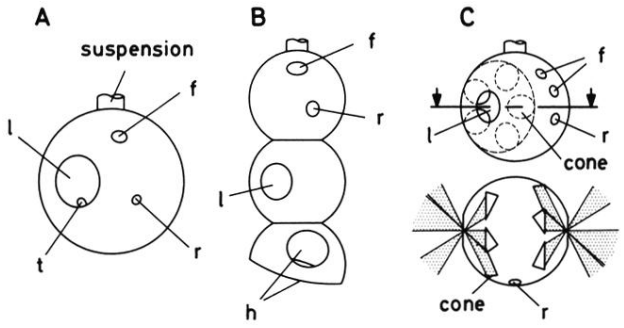

FIG. 3. Cavities of types $A-C$ used in the experiments. Small letters denote the holes with the foil (f), the open reference holes (r), the laser holes (l), the holes for temperature measurement (t), and additional holes (h) in the lower part of the type-B cavity.

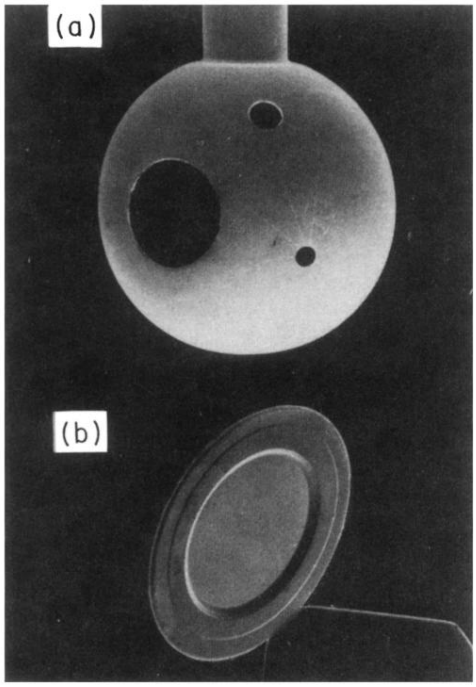

FIG. 4. (a) Scanning electron microscope (SEM) photograph of a type-A gold cavity. Cavity diameter is 2 mm. (b) SEM photograph of a gold foil reinforced by a gold ring (inner ring diameter, 250 μm). Foil and ring are still connected to a supporting foil (which holds all the 40 identical pieces fabricated on a single substrate) from which it will be cut for mounting (fabricated by Dr. Johannes Heidenhain, D-8225 Traunreut, Federal Republic of Germany).

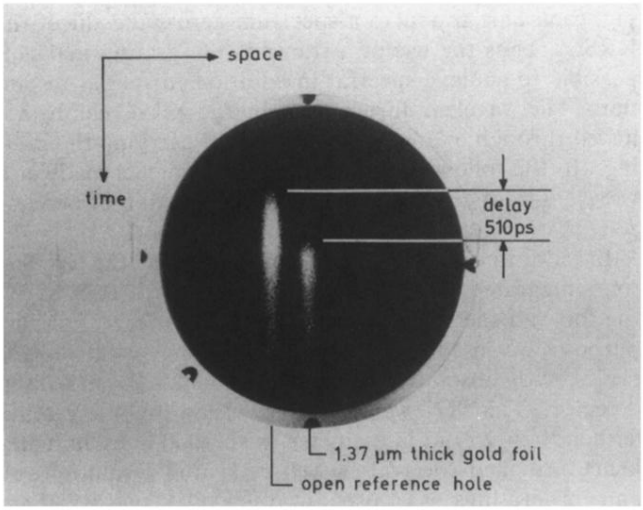

FIG. 6. Screen of the x-ray streak camera showing signals from the gold foil and the open reference hole. Observed wavelength, 60 Å. Cavity temperature, 230 eV. Fiducial marks are seen at the periphery of the screen.